Predicting the Properties of the Fallback Rate from Tidal Disruption Events: Investigating the Maximum Gravity Model

Julia Fancher[1] , Ananya Bandopadhyay[1] , Eric R. Coughlin[1] , and C. J. Nixon[2]
[1] Department of Physics, Syracuse University, Syracuse, NY 13210, USA; jlfanche@syr.edu, abandopa@syr.edu
[2] School of Physics and Astronomy, Sir William Henry Bragg Building, Woodhouse Ln., University of Leeds, Leeds LS2 9JT, UK

Abstract

A star destroyed by the tidal field of a supermassive black hole (SMBH) in a tidal disruption event (TDE) gives rise to a luminous flare. TDEs are being detected at an ever-increasing rate, motivating the need for accurate models of their lightcurves. The "maximum gravity" (MG) model posits that a star is completely destroyed when the tidal field of the SMBH exceeds the maximum self-gravitational field within the star, g_{max}, and predicts the peak fallback rate $\dot{M}_{peak}$ and the time to peak t_{peak}. Here we perform hydrodynamical simulations of the complete disruption of 24 stars with masses ranging from 0.2 to 5.0 $M_{\odot}$, at different stages of their main sequence evolution, to test the predictions of this model. We find excellent agreement between the MG model predictions and our simulations for stars near the zero-age main sequence, while the predictions are less accurate (but still within $\sim$35%–50% of the simulation results) for highly evolved stars. We also generalize the MG model to incorporate the Paczyński–Wiita potential to assess the impact of strong-gravity effects, which are especially important for deep encounters that are required to completely destroy evolved and centrally concentrated stars, and find good agreement with recent works that include relativistic gravity. Our results demonstrate that this model provides accurate constraints on the peak timescale of TDE lightcurves and their correlation with black hole mass.

Unified Astronomy Thesaurus concepts: Astrophysical black holes (98); Supermassive black holes (1663); Black hole physics (159); Tidal disruption (1696); Hydrodynamics (1963)

1. Introduction

A tidal disruption event (TDE) occurs when a star is partially or completely destroyed by the tidal field of a supermassive black hole (SMBH; J. G. Hills 1975; M. J. Rees 1988; S. Gezari 2021). Approximately half of the tidally stripped debris is bound to the black hole and circularizes to form an accretion disk (J. K. Cannizzo et al. 1990; A. Loeb & A. Ulmer 1997; K. Hayasaki et al. 2013; E. R. Coughlin & M. C. Begelman 2014; H. Shiokawa et al. 2015; C. Bonnerot et al. 2016; A. Sadowski et al. 2016; B. Curd & R. Narayan 2019; Z. L. Andalman et al. 2022; E. Steinberg & N. C. Stone 2024; M. R. Meza et al. 2025). The process of accretion releases energy at a rate comparable to or in excess of the Eddington limit of the SMBH (C. R. Evans & C. S. Kochanek 1989; S. Wu et al. 2018), seen in the form of a luminous electromagnetic flare with—at least in some cases— associated outflows (J. S. Bloom et al. 2011; S. B. Cenko et al. 2012; G. C. Brown et al. 2015; J. M. Miller et al. 2015; K. D. Alexander et al. 2016; D. R. Pasham & S. van Velzen 2018; I. Andreoni et al. 2022; D. R. Pasham et al. 2023, 2024; T. Wevers et al. 2024; Y. Ajay et al. 2025). The detection rate of these flares has increased steadily in the past years (I. Arcavi et al. 2014; K. D. French et al. 2016; M. Nicholl et al. 2019, 2022; D. R. Pasham et al. 2019; T. Wevers et al. 2019, 2021, 2023; J. T. Hinkle et al. 2021; A. V. Payne et al. 2021; S. van Velzen et al. 2021; Z. Lin et al. 2022; E. Hammerstein et al. 2023; Y. Yao et al. 2023; M. Guolo et al. 2024; A. Y. Q. Ho et al. 2025; see also

S. Gezari 2021 and references therein), and with the advent of the Vera Rubin Observatory (Ž. Ivezić et al. 2019) will increase further.

The fallback rate $\dot{M}$, or the rate at which the stellar material returns to the SMBH, is the main factor in determining the properties of the accretion disk in the first few years of disk formation (M. J. Rees 1988; J. K. Cannizzo et al. 1990; G. Lodato & E. M. Rossi 2011). Analytic models of the fallback rate of a TDE are thus useful in characterizing these systems, the earliest example of which is known as the frozen approximation (B. Carter & J. P. Luminet 1982; J. H. Lacy et al. 1982; G. V. Bicknell & R. A. Gingold 1983; N. Stone et al. 2013). This model assumes that the star is completely and instantaneously destroyed as it passes through the sphere of radius r_t from the SMBH, where r_t—the tidal radius—is determined by equating the surface gravitational field of the star with the tidal acceleration due to the SMBH, which yields (J. G. Hills 1975)

$$r_t = R_\star \left(\frac{M_\bullet}{M_\star} \right)^{1/3}. \tag{1}$$

Here $M_\bullet$ is the mass of the SMBH and $M_\star$ and $R_\star$ are the stellar mass and radius, respectively. In this model, the peak of the fallback rate and the time to peak (see Section 2.2 below for examples) are determined by the bulk properties of the star and the canonical tidal radius r_t (as defined in Equation (1)), and are strongly dependent on stellar type (see G. Lodato et al. 2009, and in particular their generalization to include the stellar density profile; see also M. Gallegos-Garcia et al. 2018). While this model's predictions are in reasonable agreement with numerical simulations of the disruption of low-mass and polytropic stars (J. H. Lacy et al. 1982; C. R. Evans & C. S. Kochanek 1989; G. Lodato et al. 2009), the predictions

for higher-mass stars are highly discrepant (and even inverted, i.e., the model predicts that the fallback rate for the disruption of a solar-like star peaks at a later time and at smaller magnitude compared to a low-mass star, while the opposite is observed in simulations; E. C. A. Golightly et al. 2019), and the strong dependence of the fallback rate on stellar properties predicted by this model is generally not found (A. Bandopadhyay et al. 2024b).

These discrepancies have been noted by, e.g., J. Guillochon & E. Ramirez-Ruiz (2013), F. G. Goicovic et al. (2019), E. C. A. Golightly et al. (2019), J. Law-Smith et al. (2019), J. A. P. Law-Smith et al. (2020), T. Ryu et al. (2020a), T. Janković & A. Gomboc (2023). Some of these investigations generated empirical (i.e., based on the results of numerical experiments) scalings for the impact parameter $\beta \equiv r_t/r_p$ (where r_p is the pericenter distance) at which a star is completely destroyed, denoted β_c, and the corresponding distance $r_{t,c}$. For example, J. A. P. Law-Smith et al. (2020) found that the critical impact parameter scales as $\beta_c \sim 0.5 (\rho_c/\rho_\star)^{1/3}$, where ρ_c ($\rho_\star$) is the central (average) stellar density, for stars having $\rho_c/\rho_\star \lesssim 500$, while $\beta_c \sim 0.39 (\rho_c/\rho_\star)^{1/2.3}$ when $\rho_c/\rho_\star \gtrsim 500$. T. Ryu et al. (2020b) also found that $\beta_c \propto (\rho_c/\rho_\star)^{1/3}$.

These scalings were based on simulations of TDEs. In contrast, E. R. Coughlin & C. J. Nixon (2022) proposed that a star is completely destroyed if the tidal field of the SMBH exceeds the maximum self-gravitational field that occurs at some nonzero radius in the stellar interior (denoted the "core radius," R_c), which is always greater than the surface gravity. Using this definition of the core radius, they predicted the distance from the SMBH at which a star is completely destroyed, and derived analytical expressions for the peak fallback rate $\dot{M}_{peak}$ and the time at which $\dot{M}_{peak}$ is reached, t_{peak} (which can be evaluated for any stellar density profile). This model, which we refer to as the maximum-gravity (MG) model, does not make any approximations specific to stellar type, e.g., based on the ratio of $\rho_c/\rho_\star$. Nonetheless, they showed that if one extrapolates the $\propto r$ behavior of the self-gravitational field from the stellar center and the $\propto 1/r^2$ behavior from the surface, the radius at which the two intersect yields an approximation for the core radius and the aforementioned and empirically obtained scaling $\beta_c \propto (\rho_c/\rho_\star)^{1/3}$.

While E. R. Coughlin & C. J. Nixon (2022) noted the accuracy of this model when compared to extant numerical results and A. Bandopadhyay et al. (2024b) directly tested it against a handful of hydrodynamical simulations, it has not been vetted over a wide range of stellar progenitors. The aims of this work are: (1) to analyze the accuracy of the MG model when compared to numerical hydrodynamical simulations of the disruption of a wide range of stars in terms of their mass and age; (2) assess whether the approximate solution for $r_{t,c}$ coupled with the expression for t_{peak} yields good agreement with the numerically obtained values, and if a better estimate can be obtained by using higher-order approximations for the self-gravitational field; and (3) extend the MG model to include relativistic effects. In Section 2 we provide a brief overview of the MG model, outline its predictions for the peak fallback rate from TDEs, and test the predictions of the MG model against numerical hydrodynamical simulations. We find excellent agreement between the MG model predictions and the numerical results for stars near the zero-age main sequence (ZAMS), while more highly evolved and centrally
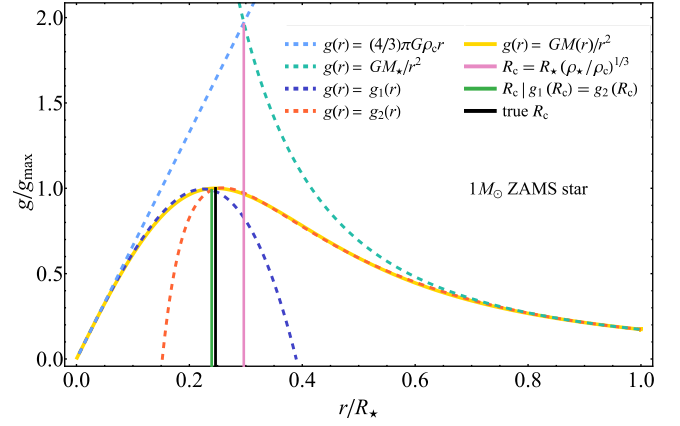
Figure 1. The self-gravitational field $g(r)$ (yellow) of a 1.0 $M_\odot$ ZAMS star, normalized by its maximum value g_{max}. The solid black line shows the core radius R_c at which $g(r)$ is maximized. Also shown are the leading order approximations for g close to the center (blue dashed) and the surface (teal dashed) of the star, and the next-to-leading order approximations (g_1 and g_2 shown by the purple and orange dashed curves). The pink and green solid lines show the intersection of the leading order and next-to-leading order approximations, respectively, which yield estimates for the core radius R_c.

concentrated stars are not completely destroyed at the β_c predicted by the model. The fallback rates from these disruptions peak at later times and with smaller magnitudes than predicted, but are still generally within a few × 10% of the MG values. In Section 3 we use the Paczyński–Wiita potential (in place of the Newtonian potential) in the MG model to estimate the impact of relativistic effects, and find—despite the simplicity of this approximation—good agreement with other works. We discuss the implications of our results and conclude in Section 4.

2. Maximum Gravity Model

2.1. Predictions

The MG model postulates that a star is completely destroyed when the tidal field of an SMBH exceeds the maximum value of the self-gravitational field, g_{max}, of the star. The radius within the star at which its gravitational field is maximized is denoted as the "core radius," R_c. The location of the core radius depends on the stellar profile, and in general can be straightforwardly and numerically evaluated. However, directly solving for the core radius for a given stellar structure does not lend obvious insight into its variation with the bulk properties of a star, such as $M_\star$ and $R_\star$. Alternatively, an estimate for the core radius R_c can be obtained by using the lowest-order expansions for the gravitational field of the star near its center ($g(r) = (4/3)\pi G\rho_c r$) and surface ($g(r) = GM_\star/r^2$). E. R. Coughlin & C. J. Nixon (2022) demonstrated that setting the two equal to one another yields a parameterization of the core radius in terms of the bulk properties of the star, namely ρ_c, $M_\star$ and $R_\star$,

$$R_c = R_\star \left(\frac{\rho_\star}{\rho_c}\right)^{1/3}, \qquad (2)$$

where $\rho_\star = 3M_\star/4\pi R_\star^3$ is the average stellar density. Figure 1 shows the lowest-order approximations for $g(r)$ and the approximate core radius R_c (given by Equation (2)) at which the two curves intersect, for a 1 $M_\odot$ ZAMS star, in relation to

their exact values as obtained from the MESA (B. Paxton et al. 2011) profile. As seen in the figure, the approximate curves intersect at a larger radius than the true core radius, and yield a g_{max} that is about twice its true value.

We can obtain a more accurate estimate of R_c by incorporating additional details of the stellar structure. To do so, we parameterize the approximate expressions for the self-gravitational field within the star in terms of higher-order moments of its mass distribution. The mass contained within a small volume of radius R near the center of the star can be estimated by using the Taylor expansion of the density about $R = 0$:

$$M_1(R) = 4\pi\left(\rho_c \frac{R^3}{3} - \frac{1}{2}\rho_c'' \frac{R^5}{5}\right), \qquad (3)$$

where ρ_c'' is the second derivative of the density evaluated at the center of the star, such that the self-gravitational field is

$$g_1(R) = 4\pi G\left(\rho_c \frac{R}{3} - \frac{1}{2}\rho_c'' \frac{R^3}{5}\right). \qquad (4)$$

Conversely, near the stellar surface the mass enclosed is

$$M_2(R) = M_\star\left[1 + A\left(1 - \frac{R}{R_\star}\right)^n\right], \qquad (5)$$

where A and n are constants that can be determined from the MESA-generated mass profile (for the 1 $M_\odot$ ZAMS star the best fit values are $A = -1.8$ and $n = 3.6$), such that

$$g_2(R) = \frac{GM_\star}{R^2}\left[1 + A\left(1 - \frac{R}{R_\star}\right)^n\right] \qquad (6)$$

is the corresponding self-gravitational field. The purple- and orange dashed curves in Figure 1 show the functions g_1 and g_2 for the 1 $M_\odot$ ZAMS star, and the green solid line marks the intersection of the two curves. As seen in the figure, the core radius R_c obtained from the intersection of the g_1 and g_2 curves very closely approximates the true core radius (shown by the solid black line).

The approximate expressions for the gravitational field can be used to determine the critical tidal disruption radius radius $r_{t,c}$ (i.e., the distance of closest approach at which the star would be completely destroyed by tides) by equating the tidal field of the black hole at the location of the core to the star's self-gravitational field at that location. We can then calculate the peak timescale t_{peak} and the peak fallback rate $\dot{M}_{peak}$ using Equations (11) and (12) in E. R. Coughlin & C. J. Nixon (2022). Setting the tidal field of the black hole equal to $(4/3)\pi G\rho_c R_c$ (the lowest-order approximate expression for the gravitational field at the core) yields, for the critical tidal radius,

$$r_{t,c} = r_t\left(\frac{\rho_c}{4\rho_\star}\right)^{-1/3}, \qquad (7)$$

where r_t is the canonical tidal radius. The peak timescale (using Equation (11) of E. R. Coughlin & C. J. Nixon 2022) then evaluates to

$$t_{peak} = \left(\frac{\rho_c}{4\rho_\star}\right)^{-1/2}\left(\frac{r_t^2}{2R_\star}\right)^{3/2}\frac{2\pi}{\sqrt{GM_\bullet}}. \qquad (8)$$
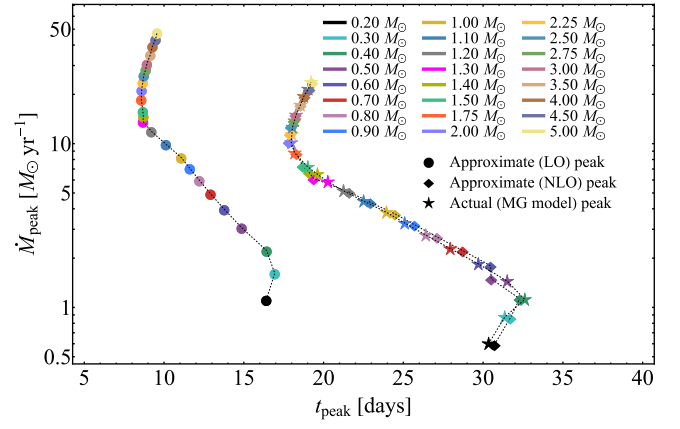
Figure 2. The peak fallback times t_{peak} and rates $\dot{M}_{peak}$ for 0.2–5 $M_\odot$ ZAMS stars disrupted by a $10^6 M_\odot$ SMBH. The five-pointed stars represent the exact MG prediction, obtained by using the true location of the core radius R_c. The circles and diamonds represent the predicted peaks using the leading order (LO) and next-to-leading order (NLO) approximations for the self-gravitational field, and the corresponding values of R_c. This demonstrates that, while the leading order expansion provides a significant improvement on the frozen-in approximation, the next terms in the expansion of the gravitational field are required to accurately predict the peak fallback rate properties.

In addition to the fallback timescale, $t_{fb} = (r_t^2/2R_\star)^{3/2}\times 2\pi/\sqrt{GM_\bullet}$ (J. H. Lacy et al. 1982), the expression for t_{peak} depends on the ratio $\rho_c/\rho_\star$ of the central density to the average stellar density. The corresponding peak fallback rates can be expressed as $\dot{M}_{peak} = M_\star/4t_{peak}$ (using Equation (12) of E. R. Coughlin & C. J. Nixon 2022).

Figure 2 shows the approximate peak timescales (depicted with circles) obtained using Equation (8), and peak fallback rates for 0.2–5 $M_\odot$ ZAMS stars, alongside the (t_{peak}, $\dot{M}_{peak}$) values obtained using the exact core radius R_c (depicted with five-pointed stars), for tidal disruption by a $10^6 M_\odot$ SMBH. As seen in the figure, the approximate expression for t_{peak} underpredicts its true value by a factor of ~2–3 for the ZAMS stars, and overpredicts $\dot{M}_{peak}$. A. Bandopadhyay et al. (2024b) showed that the peak timescale is roughly independent of stellar mass and age, and for a $10^6 M_\odot$ SMBH, ranges between ~15 and 30 days. We can thus infer that the approximate peak timescale given by Equation (8), which scales as $\propto(\rho_c/4\rho_\star)^{-1/2}$, becomes increasingly discrepant for highly evolved stars, for which the ratio of the central density to the average density increases.

Figure 2 also shows the approximate t_{peak} and $\dot{M}_{peak}$ obtained using the next-to-leading order approximations for the self-gravitational field for the same range of stars. The agreement between the higher-order-approximated t_{peak} and $\dot{M}_{peak}$ and the exact values (i.e., using the exact values of R_c and $r_{t,c}$) indicates that higher-order moments of the mass distribution of a star are necessary to accurately parameterize the peak fallback properties. Conversely, accurately predicting the peak fallback rate properties cannot be achieved with only ρ_c, $M_\star$ and $R_\star$. While this demonstrates the need for additional parameters to accurately model the peak of the fallback rate, it is more straightforward to simply use the exact values of R_c and $r_{t,c}$; in Section 2.2 we compare these values to those obtained from numerical simulations of TDEs.

2.2. Numerical Simulations

We test the MG model by running multiple sets of numerical simulations of TDEs. We evolve stars with masses
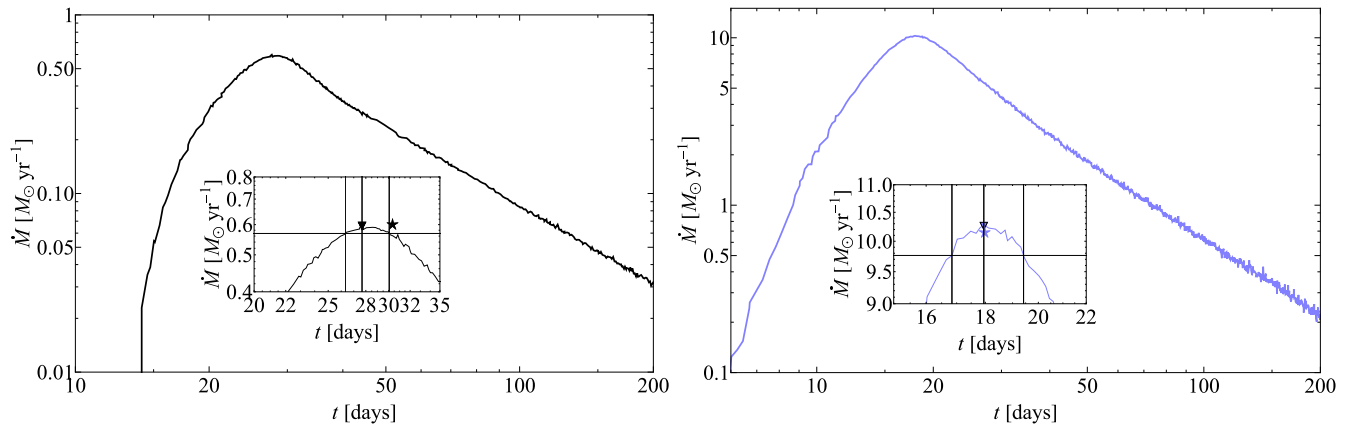
Figure 3. The fallback curves following the disruption of a 0.2 $M_\odot$ ZAMS star (left) and a 2.0 $M_\odot$ ZAMS star (right) by a $10^6 \, M_\odot$ SMBH. The insets zoom in on the peak, where the inverted triangle shows the numerical peak value and the star marks the MG model prediction. The horizontal line shows 95% of the peak value, and the vertical lines show the time at which the fallback rate reaches 95% of the peak value, represented in Figure 4 as the error bars.

ranging from 0.2 to 5.0 $M_\odot$ through the main sequence using MESA (B. Paxton et al. 2011). The stellar profiles are then imported into the smoothed particle hydrodynamics code PHANTOM (D. J. Price et al. 2018), where they are relaxed for approximately five sound crossing times using the routine implemented in E. C. A. Golightly et al. (2019) and C. J. Nixon et al. (2021). We use a resolution of 10^6 particles to model the stars in PHANTOM. We simulate the disruption of stars by a $10^6 \, M_\odot$ SMBH modeled as a Newtonian point mass potential, with the relaxed MESA star initially placed at a distance of $5r_t$ on a parabolic Keplerian orbit with pericenter $r_{t,c} = r_t/\beta_c$, with β_c determined from the MG model. We run three sets of simulations of 24 stars in the mass range 0.2–5.0 $M_\odot$. The three sets are at different ages: ZAMS, terminal-age main sequence (TAMS), and "middle-age main sequence" (MAMS), defined as the time at which the central hydrogen mass fraction falls below 0.2. We do not simulate MAMS and TAMS stars with masses below 0.9 $M_\odot$, as stars of these masses would not reach MAMS or TAMS in the age of the Universe.

The fallback rates are calculated directly in PHANTOM by counting particles as they pass into the accretion radius of the SMBH (we find that the bin size used to calculate the fallback rate does not significantly impact the peak magnitude or peak timescale). Approximately one day after the star passes pericenter, the accretion radius is increased to 120 gravitational radii (E. R. Coughlin & C. Nixon 2015; E. C. A. Golightly et al. 2019). If a core reforms within that same time period, the core is replaced by a sink particle, which is a good approximation for the core (for more detail, see P. R. Miles et al. 2020; C. J. Nixon et al. 2021; A. Bandopadhyay et al. 2024a).

The directly calculated fallback rates for a 0.2 $M_\odot$ (left) and a 2.0 $M_\odot$ star at ZAMS (right) are shown in Figure 3. The inset shows a zoomed-in view of the peak, where the numerical peak is marked with an inverted triangle. The MG prediction is marked with a star. The horizontal line delimits where the fallback rate is 95% of its peak magnitude, and the outer vertical lines mark the times at which the fallback rate is 95% of the peak value. The central vertical line marks the time at which the peak occurs. The MG prediction for the 0.2 $M_\odot$ ZAMS star falls slightly outside the 95% interval because the peak is much shallower, and slight numerical noise has influenced the value chosen as the peak.

Figure 4 shows the comparison between the predicted peak fallback rate of the MG model (shown as stars) and the numerical peak fallback rate from the set of simulations using ZAMS stars (shown as inverted triangles), where the color represents the mass of the star. The error bars mark the duration of time for which the fallback rate is above 95% of its peak value, as shown by the insets of Figure 3. The numerical values thus agree extremely well with the MG prediction over the entire mass range.

Figure 5 shows the results from simulations of MAMS (left) and TAMS (right) stars compared with the MG model predictions. The error bars, as in Figure 4, mark the duration for which the fallback rate is above 95% of $\dot{M}_{\rm peak}$. It is clear that the model is less accurate for evolved stars, and the discrepancy between the prediction and the numerically obtained results increases as mass and age increase. Nonetheless, the MG model is still considerably more accurate than the frozen-in approximation, which overestimates the peak timescale by months to years and underestimates the peak fallback rate by up to two orders of magnitude for the highest-mass stars (E. C. A. Golightly et al. 2019; A. Bandopadhyay et al. 2024b).

There are two possible origins[3] for the discrepancy between the predictions of the MG model and the PHANTOM fallback rates from evolved stars. First, if the disruption is only partial, the presence of a core modifies the debris dynamics (J. Guillochon & E. Ramirez-Ruiz 2013; E. R. Coughlin & C. J. Nixon 2019), and a core reforms almost immediately after pericenter for the MAMS and TAMS stars. Figure 6 shows the fallback rates of a 2.0 $M_\odot$ star at MAMS (left) and TAMS (right), where the insets are the same as in Figure 3, but the MG model predictions are shown by the clover and spade, respectively. The fallback rates exhibit a $t^{-9/4}$ scaling (the black dashed line in the figure shows a $\propto t^{-9/4}$ power law) at late times, appropriate to the case of a partial disruption (E. R. Coughlin & C. J. Nixon 2019). The MG model assumes that the star is completely destroyed, and is hence less accurate for the case of these partial disruptions.

---

[3] In addition to the two physical origins we describe, a third possibility could be related to a lack of numerical convergence, but we directly demonstrate in the Appendix that our results are strongly converged, especially near the peak in the fallback rate.
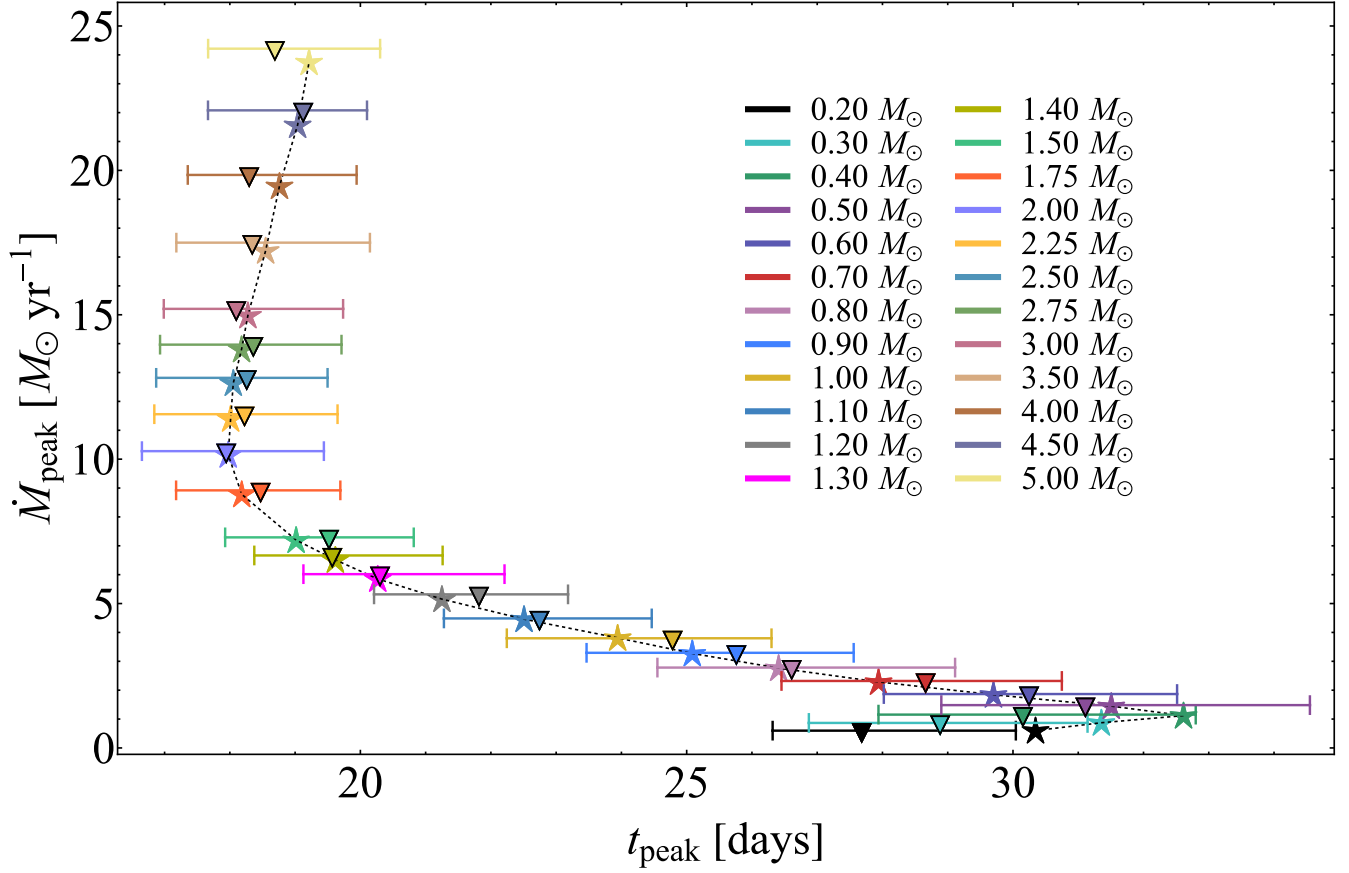
Figure 4. The predictions of the MG model for the disruption of ZAMS stars at varying masses (stars) compared to the numerical value of the peak fallback rate (triangles). The horizontal lines provide the amount of time for which the fallback rate is above 95% of its peak value; see the insets in Figures 3 and 6 for examples.
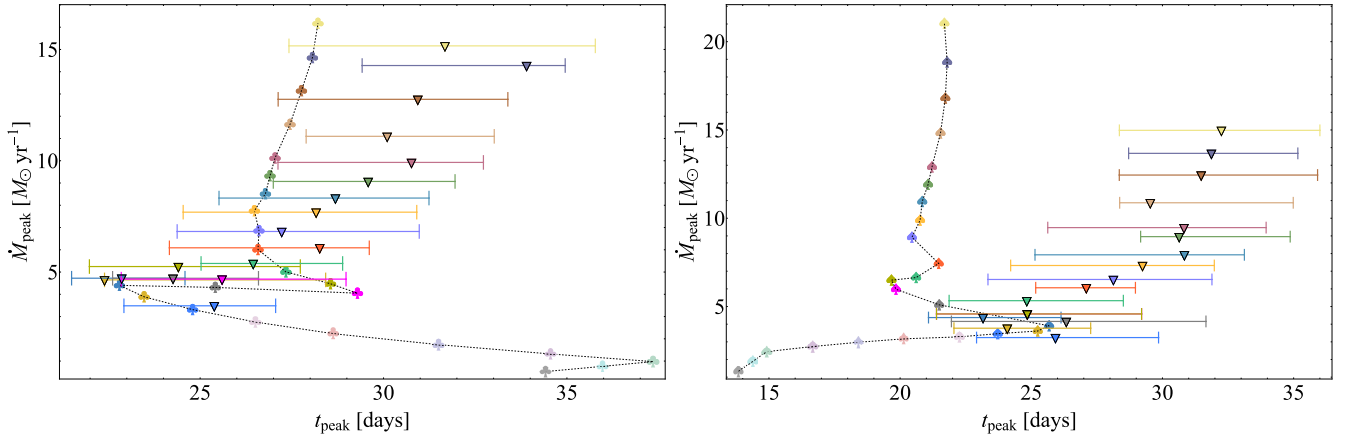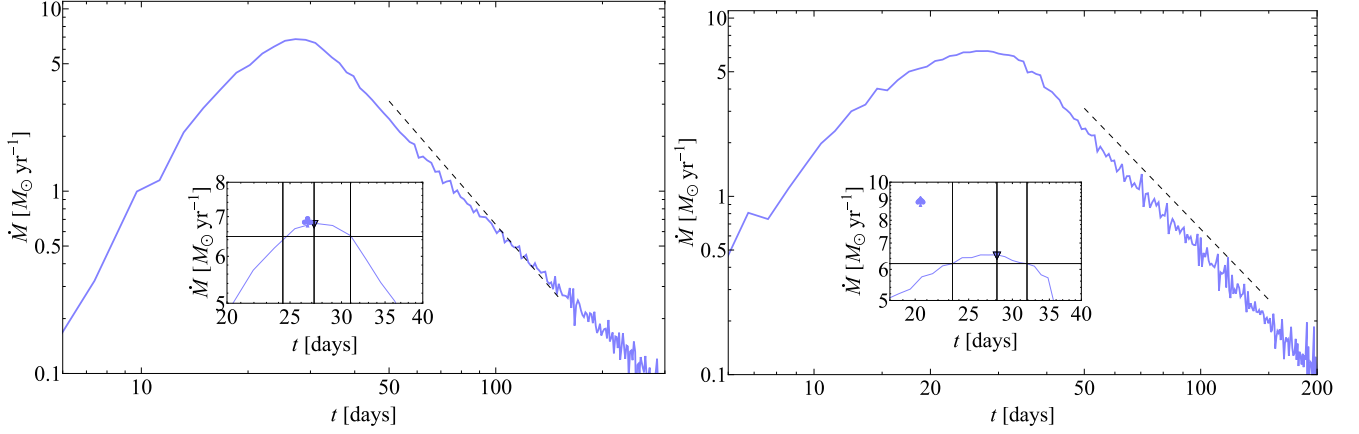

Figure 5. Same as Figure 4 but for the disruption of MAMS (left) and TAMS (right) stars.

Alternatively, the core radius itself may differ from the model prediction, which could be due to the tidal compression of the star and the resultant increase in the central density and self-gravitational field.[4] In particular, the MG model assumes that the maximum self-gravitational field against which the tidal field competes is established by the original density profile of the star, but for deep encounters which are required

to completely destroy high-mass and evolved stars the central density (and self-gravitational field) is augmented by the vertical component of the SMBH tidal field (B. Carter & J. P. Luminet 1982), thus making the core more capable of withstanding the tidal shear (and making the core radius smaller). A smaller R_c than predicted would yield a longer peak timescale (using Equation (11) of E. R. Coughlin & C. J. Nixon 2022) and, correspondingly, a smaller $\dot{M}_{\rm peak}$. To test which of these possibilities—the reformed core or a smaller R_c—is more responsible for modifying the values from their MG predictions, we performed additional simulations at $\beta = \beta_c + 1$, and found that the MAMS stars are completely

---

[4] In support of the fact that self-gravity is significantly increased in deep encounters, C. J. Nixon & E. R. Coughlin (2022) found that a 5/3 polytropic star is completely destroyed by a $10^6\ M_\odot$ SMBH for $\beta = 8$, while a core reforms for $\beta = 16$.

Figure 6. Same as Figure 3, but for the disruption of a 2.0 $M_\odot$ star at MAMS (left) and TAMS (right). The black dashed line shows a scaling of $t^{-9/4}$, demonstrating that these are partial disruptions.

destroyed at $\beta_c + 1$ (with the exception of the 0.9 $M_\odot$ MAMS star, which is still partially disrupted). Despite not having a core, these disruptions still yield fallback rates with longer peak timescales and lower peak magnitudes compared to the model predictions. This finding suggests that the core radius is smaller than that predicted by the MG model and is primarily responsible for introducing the discrepancies present in Figure 5, but that the β_c predicted by the model is still accurate.

Because the tidal compression strengthens the self-gravitational field, it may be impossible to completely destroy high-mass TAMS stars with a Newtonian tidal field. However, this resistance to disruption may be unphysical, because relativistic effects (which strengthen the tidal field of the black hole) become more pronounced at such high β's. In Section 3 we construct a simple relativistic generalization of the MG model to address the importance of such effects.

3. Relativistic Generalization

The analytical model developed in E. R. Coughlin & C. J. Nixon (2022) treats the SMBH as a Newtonian point mass potential. For a Sunlike star ($M_\star = 1\ M_\odot$; $R_\star = 1\ R_\odot$) being disrupted by a $10^6\ M_\odot$ SMBH, the ratio of the tidal radius r_t to the gravitational radius $r_g = GM_\bullet/c^2$ of the SMBH is ~ 50. The length scales involved in this system thus justify the Newtonian approximation, and a general relativistic treatment would yield minor corrections to t_{peak} and $\dot{M}_{peak}$, as demonstrated by E. Gafton & S. Rosswog (2019). However, the ratio r_t/r_g scales as $\propto M_\bullet^{-2/3}$, and is thus increasingly non-ignorable as the SMBH mass grows.

Here we estimate the importance of relativistic effects in modifying the tidal field of an SMBH by using the Packzyński–Wiita potential (B. Paczyński & P. J. Wiita 1980),

$$\Phi_\bullet = -\frac{GM_\bullet}{r - 2r_g}, \tag{9}$$

where $M_\bullet$ is the SMBH mass, and $r_g = GM_\bullet/c^2$ is its gravitational radius, in place of the Newtonian potential used in E. R. Coughlin & C. J. Nixon (2022). For the complete disruption of a star, the tidal field evaluated at its core radius R_c must exceed the self-gravitational field of the core, $g(R_c)$.

This yields, for the critical disruption radius $r_{t,c}^{PW}$,

$$\frac{4GM_\bullet R_c}{(r_{t,c}^{PW} - 2r_g)^3} = g(R_c) \Rightarrow r_{t,c}^{PW} = 2r_g + \left(\frac{4GM_\bullet R_c}{g(R_c)}\right)^{1/3}, \tag{10}$$

where the second term on the right-hand side of the second equality is the Newtonian $r_{t,c}$. This shows that the tidal field of the SMBH is stronger than its Newtonian estimate, thus resulting in a larger complete disruption radius. Equation (10) can be used to define the relativistic analog of the critical impact parameter required for the complete disruption of a star:

$$\beta_c^{PW} = r_t/r_{t,c}^{PW}. \tag{11}$$

The left panel of Figure 7 shows the critical impact parameter required for the complete disruption of 0.2–5 $M_\odot$ ZAMS stars by SMBHs ranging from 10^5–$10^7\ M_\odot$, alongside the Newtonian estimate for β_c (which is independent of SMBH mass), while the right panel gives the ratio $\beta_c^{PW}/\beta_c^{NR}$. Since the relativistic tidal field is stronger for a more massive SMBH, the minimum distance within which a star must approach to be destroyed by tides is larger, thus yielding a smaller β_c^{PW} for higher-mass SMBHs. For all three SMBH masses shown in the figure, β_c reaches a maximum at $M_\star = 1.4\ M_\odot$. This peak is due to the fact that β_c is strongly correlated with the "compactness" of a star, defined as the ratio of the core radius R_c to the stellar radius $R_\star$. Specifically, since the canonical tidal radius $r_t = R_\star \times (M_\bullet/M_\star)^{1/3}$, while the critical disruption radius $r_{t,c} = R_c \times (4M_\bullet/M_c)^{1/3}$ (where M_c is the core mass), $\beta_c \equiv r_t/r_{t,c} \propto (R_\star/R_c) \times (M_\star/M_c)^{-1/3}$. The core mass fraction $M_c/M_\star$ is ~ 1 if one approximates the density of the core as equal to ρ_c out to R_c (E. R. Coughlin & C. J. Nixon 2022), and thus has a relatively minor influence on the variation in β_c compared to the compactness parameter. The fact that β_c has a relative maximum at $M_\star = 1.4\ M_\odot$ thus arises primarily from the fact that this star has the smallest value of $R_c/R_\star$ among all the ZAMS stars. The left and right panels of Figure 8 are analogous to the left panel of Figure 7, but for MAMS and TAMS stars.

The estimate for the critical impact parameter β_c^{PW} at which a star is completely destroyed is in good agreement with numerical simulations of TDEs that account for general
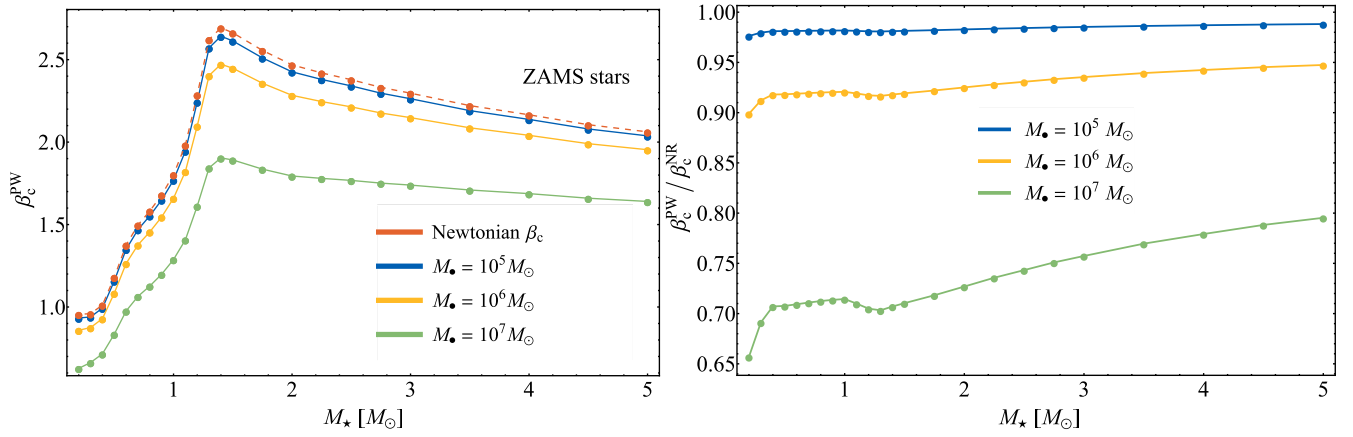
Figure 7. Left: the critical impact parameter β_c^{PW} obtained using the Packzyński−Wiita potential, as a function of stellar mass, for zero-age main-sequence stars disrupted by SMBHs of masses 10^5, 10^6, and 10^7 $M_\odot$ (represented by the blue, yellow, and green lines, respectively). The orange dashed curve shows the β_c estimated using the Newtonian potential for the tidal field of the SMBH (identical to the ZAMS curve in the left panel of Figure 4 of A. Bandopadhyay et al. 2024b), which is independent of the SMBH mass. Right: the ratio of β_c for the Packzyński–Wiita potential (β_c^{PW}) to the nonrelativistic value (β_c^{NR}), for the same range of ZAMS stars and three different SMBH masses.
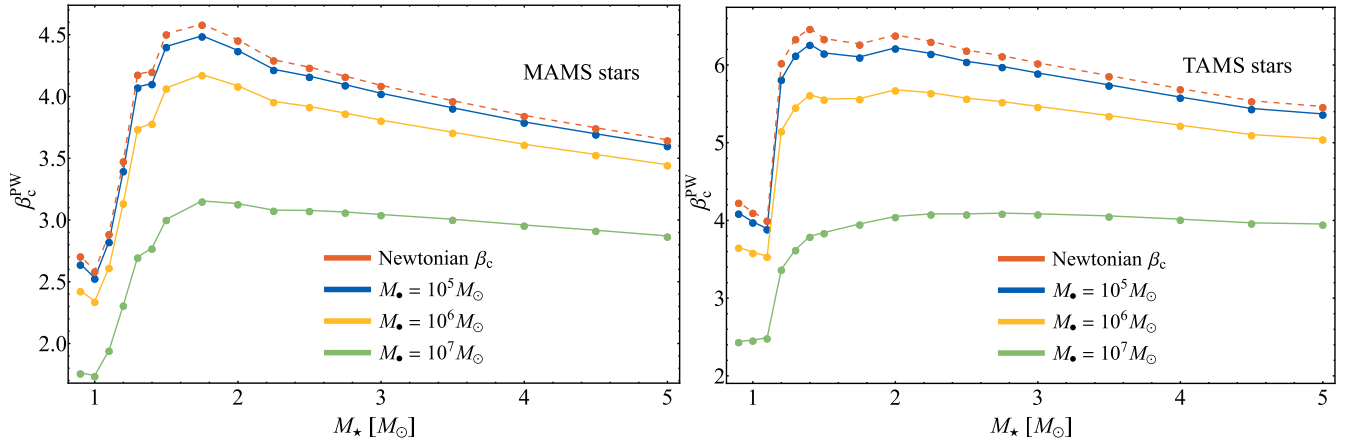

Figure 8. Same as Figure 7, but for the disruption of middle-age main sequence (left) and terminal-age main sequence (right) stars.

relativistic effects (e.g., E. Gafton et al. 2015; E. Gafton & S. Rosswog 2019; T. Ryu et al. 2020c; T. Jankovič & A. Gomboc 2023). Specifically, for the ZAMS stars shown in Figure 7, the estimates for β_c^{PW} are approximately equal to the values of β in Figure 2 of T. Jankovič & A. Gomboc (2023) at which the star is completely destroyed. Figure 9 shows a comparison of the critical impact parameter (using Equation (11)) required for the complete disruption of a Sunlike star modeled as a 5/3 polytrope (solid blue curve), as a function of the SMBH mass, and the corresponding results from Figure 3 of E. Gafton et al. (2015) (green dashed curve), who simulated the disruption of a 5/3 polytropic star for a range of impact parameters and black hole masses. They used the generalized Newtonian potential derived in E. Tejeda & S. Rosswog (2013) to model the relativistic effects for a Schwarzschild black hole. As seen in the figure, the prediction obtained using the Packzyński–Wiita potential is in good agreement with the numerical results for black hole masses $M_\bullet \sim 10^6$–10^7 $M_\odot$. There is a larger discrepancy between the β_c predicted using this generalization for the MG model and the E. Gafton et al. (2015) result for 4×10^7 $M_\odot$, but for this SMBH mass, the pericenter distance is $\sim 6 r_g$ and therefore highly relativistic, where the Packzyński–Wiita potential does

not provide an accurate enough description of relativistic gravity.

4. Discussion and Conclusions

The TDE fallback rate—the rate at which tidally stripped material returns to the disrupting black hole—has been the subject of extensive analytical and numerical modeling. Here we performed hydrodynamical simulations to test the predictions of the maximum-gravity (MG) model, which was proposed in E. R. Coughlin & C. J. Nixon (2022) and uses the core radius R_c, being the location in the tidally destroyed star where its self-gravitational field is maximized, to predict the peak properties of the fallback rate. The predicted peak timescale t_{peak} and peak fallback rate $\dot{M}_{peak}$ agree exceptionally well with the results of numerical simulations for the complete disruption of ZAMS stars (as shown in Figure 4), and are less accurate (but still within $\sim 35\%$–50%) for highly centrally concentrated and evolved stars, which have longer peak timescales and (correspondingly) smaller peak fallback rates than predicted. In contrast, the frozen-in approximation (G. Lodato et al. 2009) predicts peak timescales and peak fallback rates that are discrepant by $\gtrsim 2$ orders of magnitude for the same stars (see Figure 1 of A. Bandopadhyay et al. 2024b). We also provided a relativistic generalization of the
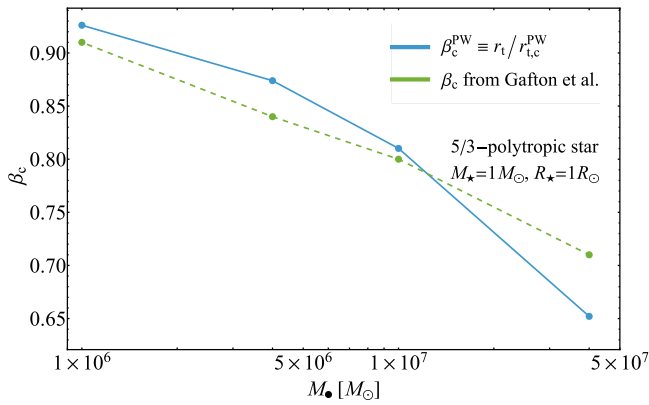
Figure 9. The critical impact parameter predicted using the Packzyński–Wiita potential, required for the complete disruption of a Sunlike star modeled as a 5/3 polytrope (blue curve), as a function of SMBH mass, $M_\bullet$. Also shown are the results of numerical simulations performed in E. Gafton et al. (2015) (green curve) using the generalized Newtonian potential from E. Tejeda & S. Rosswog (2013) to account for relativistic effects. The points on the green curve correspond to the value of β at which the core mass fraction goes to zero in Figure 3 of E. Gafton et al. (2015).

MG model, obtained by replacing the Newtonian gravitational potential with the Paczyński–Wiita potential.

The numerical simulations performed in this work are in good agreement with those of previous investigations of the complete disruption of main-sequence stars by SMBHs. F. G. Goicovic et al. (2019) used the moving-mesh code AREPO (V. Springel 2010) to study the disruption of a 1 $M_\odot$ ZAMS star by a $10^6 M_\odot$ SMBH, and found a critical impact parameter $\beta_c \sim 1.8$, and a comparable estimate for t_{peak} and $\dot{M}_{peak}$ to the ones shown here in Figure 4. E. C. A. Golightly et al. (2019) simulated the disruption of three MESA evolved stars, with masses 0.3 $M_\odot$, 1 $M_\odot$, and 3 $M_\odot$ at three different ages along the main sequence. They performed simulations for a single impact parameter $\beta = 3$, and noted that the high-mass and evolved stars (specifically the 1 $M_\odot$ TAMS star and the 3 $M_\odot$ MAMS and TAMS stars) were not completely destroyed at $\beta = 3$, which is in agreement with the $t^{-9/4}$ scaling that we find here for the same stars (and at $\beta_c > 3$ for all three stars).

J. A. P. Law-Smith et al. (2020) performed simulations of the disruption of main-sequence stars with masses ranging from ~0.1 to 10 $M_\odot$ by a $10^6 M_\odot$ SMBH, using the Eulerian code FLASH (B. Fryxell et al. 2000). The critical impact parameters at which they found complete disruption of ZAMS stars, as well as the peak timescale and peak magnitude of the corresponding fallback rates, are in good agreement with the results of the PHANTOM simulations presented here (and, hence, with the MG model). They noted that the highly centrally concentrated TAMS stars (specifically, the 1.0 $M_\odot$ and 1.5 $M_\odot$ TAMS stars) did not get destroyed at the maximum β encounters simulated in their work, and extrapolated their scaling for the critical β (based on the ratio of the central density to the average density, and obtained as an empirical fit to the results of the numerical simulations) to conclude that the critical impact parameter for complete disruption should be $\beta_c = 7.0$ and $\beta_c = 10.0$ for the 1.0 $M_\odot$ and 1.5 $M_\odot$ TAMS stars respectively (the highest impact parameters for their simulations being $\beta = 6$ and $\beta = 6.7$, for which, as shown in their Figure 7, the fallback rates exhibit the same scaling as the partial disruptions). For the 3 $M_\odot$ TAMS star, they find $\beta_c = 8.5$.

T. Ryu et al. (2020a) performed general relativistic hydrodynamic simulations of the disruption of MESA evolved stars, with masses ranging from 0.15 to 10.0 $M_\odot$, for six SMBH masses between 10^5 and $5 \times 10^7 M_\odot$. Since their simulations accounted for relativistic effects, they found smaller critical impact parameters for any given star compared to the predictions of the Newtonian MG model. Here, we provide a simple analytical extension of the MG model to account for relativistic effects by using the Paczyński–Witta potential to model the tidal field of the SMBH. We find good agreement between the critical impact parameters estimated using this approach and those reported in numerical investigations of TDEs that include relativistic effects, either by using a generalized Newtonian potential (e.g., E. Gafton et al. 2015; E. Gafton & S. Rosswog 2019) or by using relativistic hydrodynamics codes (e.g., T. Ryu et al. 2020c; T. Jankovič & A. Gomboc 2023). Among these works, E. Gafton et al. (2015), E. Gafton & S. Rosswog (2019) used a $\gamma = 5/3$ polytropic structure to model the disrupted star, whereas T. Ryu et al. (2020c) and T. Jankovič & A. Gomboc (2023) considered stellar structures obtained using MESA. T. Ryu et al. (2020c) simulated the disruption of three stars ($M_\star = 0.3, 1.0, 3.0 M_\odot$) at half their main-sequence lifetime, for a range of SMBH masses. T. Jankovič & A. Gomboc (2023) simulated four stellar masses, $M_\star = 0.6, 1, 2, 3 M_\odot$ at the ZAMS and TAMS stages, for $M_\bullet = 10^6 M_\odot$ and a range of SMBH spins. We compared the predictions obtained using the Paczyński–Witta potential to their simulations for nonspinning black holes, and found good agreement in the critical β for complete disruption for the ZAMS stars. For the TAMS stars, the estimate for β_c obtained using the Paczyński–Witta potential is systematically smaller than the values found in T. Jankovič & A. Gomboc (2023). However, we note that for extreme parameters, where the stellar pericenter is $\lesssim 10$ gravitational radii (as is true for the TAMS stars), a more accurate treatment of relativistic gravity than the Paczyński–Witta potential is probably required.

While we did not perform any simulations that account for relativistic effects in this work, it is likely that the fallback rates themselves are still fairly accurate, because the larger complete disruption radius implies that the Newtonian approximation for the energy of the debris is more appropriate. The simulations performed in E. Gafton & S. Rosswog (2019) demonstrate this directly for a Sunlike 5/3 polytropic star being disrupted by a $10^6 M_\odot$ SMBH—Figure 9 in their paper shows that the time to peak and peak fallback rate are insensitive to relativistic effects near the complete disruption threshold, and in general differ by less than ~10 days. The simulations of T. Jankovič & A. Gomboc (2023) consider stars over a wider range of mass and age and show more differences (at the ~20%–30% level) between relativistic and nonrelativistic treatments, but it is not clear how large these differences are near the complete disruption threshold (as their range in β was fairly sparse). Those authors also note that different prescriptions for the self-gravitational field lead to qualitative and quantitative differences in the properties of the fallback rate, and hence, it is difficult to definitively address the accuracy of the Newtonian approximation without a firm understanding of the relativistic case.

For stars near ZAMS, the model is in excellent agreement with numerical simulations (as shown in Figure 4), while the agreement is less strong for more evolved and massive stars.

TDEs from massive stars are likely to be rarer owing to their suppression in the initial mass function (IMF) and comparatively short lifetimes, although massive-star disruptions could be more common in environments such as the Galactic Center, which is often modeled using top-heavy IMFs (L. J. Smith & J. S. Gallagher 2001; H. Bartko et al. 2010) that lead to an overrepresentation of massive stars compared to a standard Kroupa IMF (P. Kroupa 2001). Additionally, newly discovered "extreme nuclear transients" (J. T. Hinkle et al. 2025; P. Wiseman et al. 2025), which are among the most energetic transients and possess luminosities exceeding $\sim 2 \times 10^{45}$ erg s^{-1}, are also consistent with the disruption of high-mass ($M_\star \gtrsim 3\,M_\odot$) stars by high-mass ($M_\bullet \gtrsim 10^8\,M_\odot$) SMBHs. Repeating partial tidal disruption events (a class of nuclear transients that repeat on timescales of months to years), and in particular those systems that have flared many times, such as ASASSN-14ko (A. V. Payne et al. 2021) and eRASSt-J045650 (Z. Liu et al. 2024), are also most readily explained if the star being partially stripped is massive (C. Liu et al. 2023, 2025; A. Bandopadhyay et al. 2024a). Contrarily, low-mass and less evolved stars are unstable to mass transfer, and would be completely destroyed within about one to two encounters following partial disruption (M. S. Hjellming & R. F. Webbink 1987; H. Ge et al. 2010; L. Dai et al. 2013; A. Bandopadhyay et al. 2025; P. Z. Yao & E. Quataert 2025).

While these systems suggest that massive-star disruptions could be more common than might be expected from a typical IMF, the MG model is at most 30%–50% inaccurate compared to numerical simulations of such disruptions, whereas the frozen-in model is discrepant (with the same simulations) by orders of magnitude. The MG model can thus provide useful observational constraints on, e.g., the SMBH mass (which is most strongly correlated with the peak timescale compared to the stellar properties; J. Guillochon & E. Ramirez-Ruiz 2013; A. Bandopadhyay et al. 2024b) from observed TDE light-curves. Since the peak timescale in our model (and simulations) is measured relative to the pericenter passage of the star, the rise time for the light curve of an observed TDE will in general be shorter than the peak timescale predicted by the model. However, the sample of ~ 30 spectroscopically classified TDEs detected by the Zwicky Transient facility (E. Hammerstein et al. 2023) all exhibit peak timescales of ~ 30–50 days, which lie in the range of $t_{\rm peak}$ values predicted for complete disruptions caused by SMBH masses $\sim 10^6\,M_\odot$, thus upholding the predictions of the MG model. We have therefore demonstrated that the MG model provides a simple and accurate prediction of the peak fallback rate and the time at which this peak occurs, and we have extended this model to account for relativistic effects.

Appendix
Convergence of Numerical Simulations

To assess the convergence of our simulations, we performed a subset of the simulations presented in Section 2 at 10^5 and 10^7 particles, compared to the fiducial resolution of 10^6 particles used for the results presented in Section 2. Figure 10 shows the fallback rates obtained using the three different resolutions for a $0.3\,M_\odot$ ZAMS star (top left), $1.0\,M_\odot$ ZAMS star (top right), $1.0\,M_\odot$ MAMS star (bottom left), and $1.0\,M_\odot$ TAMS star (bottom right). The simulation setup is identical to the description provided in Section 2. As seen in the figure, the peak of the fallback rate is almost identical at the three different resolutions, demonstrating the numerical convergence of the results shown in Figures 4–5.
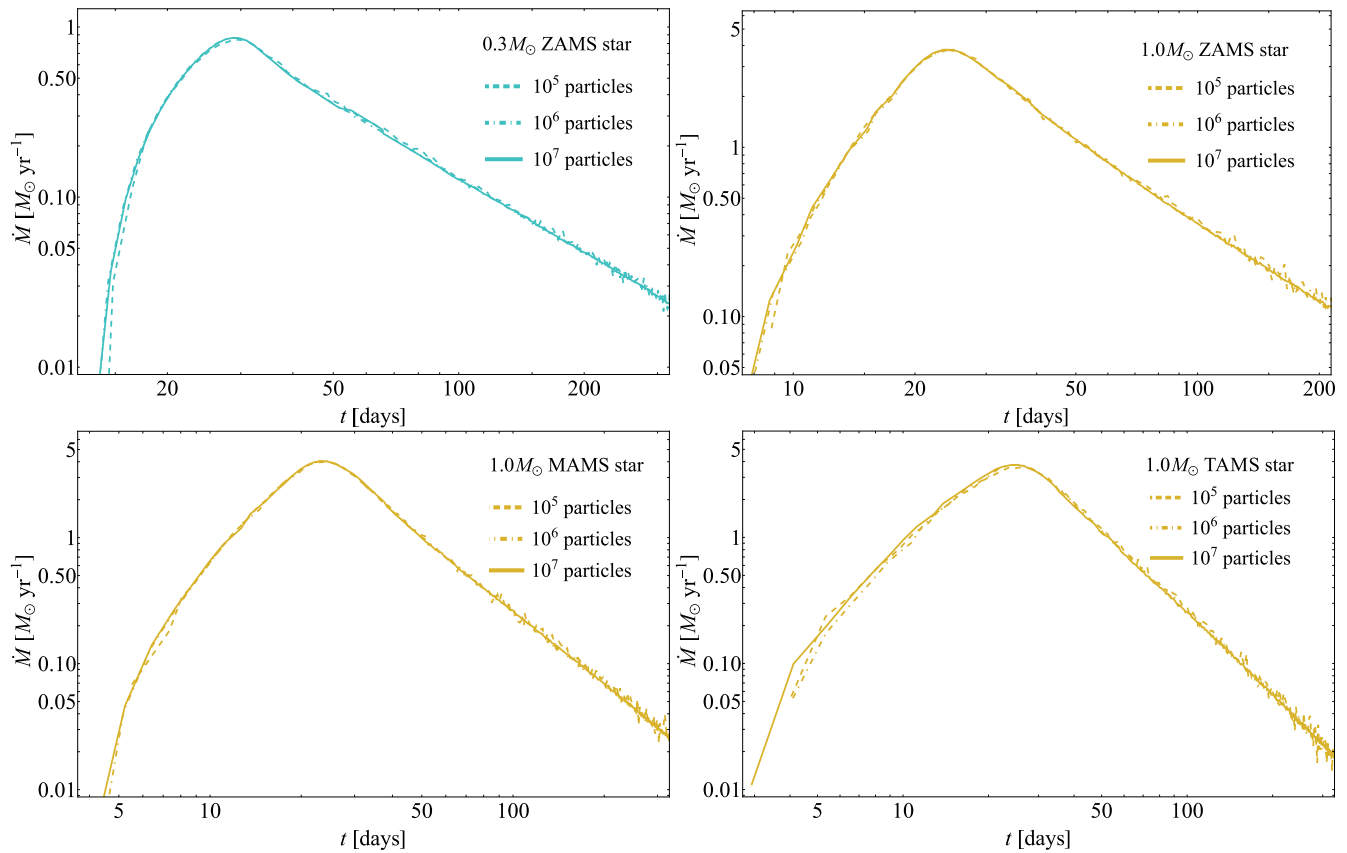
Figure 10. Fallback rates at three different numerical resolutions from the disruption of a 0.3 $M_\odot$ ZAMS star ($\beta_c = 0.96$; top left), 1.0 $M_\odot$ ZAMS star ($\beta_c = 1.80$; top right), 1.0 $M_\odot$ MAMS star ($\beta_c = 2.58$; bottom left) and 1.0 $M_\odot$ TAMS star ($\beta_c = 4.10$; bottom right), on a $\beta = \beta_c$ (as predicted by the MG model) parabolic orbit about a 10^6 $M_\odot$ SMBH.

ORCID iDs

Julia Fancher ⓘ https://orcid.org/0009-0008-5847-9778
Ananya Bandopadhyay ⓘ https://orcid.org/0000-0002-5116-844X
Eric R. Coughlin ⓘ https://orcid.org/0000-0003-3765-6401
C. J. Nixon ⓘ https://orcid.org/0000-0002-2137-4146

References

Ajay, Y., Pasham, D. R., Wevers, T., et al. 2025, ApJL, 981, L14
Alexander, K. D., Berger, E., Guillochon, J., Zauderer, B. A., & Williams, P. K. G. 2016, ApJL, 819, L25
Andalman, Z. L., Liska, M. T. P., Tchekhovskoy, A., Coughlin, E. R., & Stone, N. 2022, MNRAS, 510, 1627
Andreoni, I., Coughlin, M. W., Perley, D. A., et al. 2022, Natur, 612, 430
Arcavi, I., Gal-Yam, A., Sullivan, M., et al. 2014, ApJ, 793, 38
Bandopadhyay, A., Coughlin, E. R., & Nixon, C. J. 2025, ApJ, 987, 16
Bandopadhyay, A., Coughlin, E. R., Nixon, C. J., & Pasham, D. R. 2024a, ApJ, 974, 80
Bandopadhyay, A., Fancher, J., Athian, A., et al. 2024b, ApJL, 961, L2
Bartko, H., Martins, F., Trippe, S., et al. 2010, ApJ, 708, 834
Bicknell, G. V., & Gingold, R. A. 1983, ApJ, 273, 749
Bloom, J. S., Giannios, D., Metzger, B. D., et al. 2011, Sci, 333, 203
Bonnerot, C., Rossi, E. M., Lodato, G., & Price, D. J. 2016, MNRAS, 455, 2253
Brown, G. C., Levan, A. J., Stanway, E. R., et al. 2015, MNRAS, 452, 4297
Cannizzo, J. K., Lee, H. M., & Goodman, J. 1990, ApJ, 351, 38
Carter, B., & Luminet, J. P. 1982, Natur, 296, 211
Cenko, S. B., Krimm, H. A., Horesh, A., et al. 2012, ApJ, 753, 77
Coughlin, E. R., & Begelman, M. C. 2014, ApJ, 781, 82
Coughlin, E. R., & Nixon, C. 2015, ApJL, 808, L11
Coughlin, E. R., & Nixon, C. J. 2019, ApJL, 883, L17
Coughlin, E. R., & Nixon, C. J. 2022, MNRAS, 517, L26
Curd, B., & Narayan, R. 2019, MNRAS, 483, 565
Dai, L., Blandford, R. D., & Eggleton, P. P. 2013, MNRAS, 434, 2940

Evans, C. R., & Kochanek, C. S. 1989, ApJL, 346, L13
French, K. D., Arcavi, I., & Zabludoff, A. 2016, ApJL, 818, L21
Fryxell, B., Olson, K., Ricker, P., et al. 2000, ApJS, 131, 273
Gafton, E., & Rosswog, S. 2019, MNRAS, 487, 4790
Gafton, E., Tejeda, E., Guillochon, J., Korobkin, O., & Rosswog, S. 2015, MNRAS, 449, 771
Gallegos-Garcia, M., Law-Smith, J., & Ramirez-Ruiz, E. 2018, ApJ, 857, 109
Ge, H., Hjellming, M. S., Webbink, R. F., Chen, X., & Han, Z. 2010, ApJ, 717, 724
Gezari, S. 2021, ARA&A, 59, 21
Goicovic, F. G., Springel, V., Ohlmann, S. T., & Pakmor, R. 2019, MNRAS, 487, 981
Golightly, E. C. A., Nixon, C. J., & Coughlin, E. R. 2019, ApJL, 882, L26
Guillochon, J., & Ramirez-Ruiz, E. 2013, ApJ, 767, 25
Guolo, M., Gezari, S., Yao, Y., et al. 2024, ApJ, 966, 160
Hammerstein, E., van Velzen, S., Gezari, S., et al. 2023, ApJ, 942, 9
Hayasaki, K., Stone, N., & Loeb, A. 2013, MNRAS, 434, 909
Hills, J. G. 1975, Natur, 254, 295
Hinkle, J. T., Holoien, T. W. S., Auchettl, K., et al. 2021, MNRAS, 500, 1673
Hinkle, J. T., Shappee, B. J., Auchettl, K., et al. 2025, SciA, 11, eadt0074
Hjellming, M. S., & Webbink, R. F. 1987, ApJ, 318, 794
Ho, A. Y. Q., Yao, Y., Matsumoto, T., et al. 2025, ApJ, 989, 54
Ivezić, Ž., Kahn, S. M., Tyson, J. A., et al. 2019, ApJ, 873, 111
Janković, T., & Gomboc, A. 2023, ApJ, 946, 25
Kroupa, P. 2001, MNRAS, 322, 231
Lacy, J. H., Townes, C. H., & Hollenbach, D. J. 1982, ApJ, 262, 120
Law-Smith, J., Guillochon, J., & Ramirez-Ruiz, E. 2019, ApJL, 882, L25
Law-Smith, J. A. P., Coulter, D. A., Guillochon, J., Mockler, B., & Ramirez-Ruiz, E. 2020, ApJ, 905, 141
Lin, Z., Jiang, N., Kong, X., et al. 2022, ApJL, 939, L33
Liu, C., Mockler, B., Ramirez-Ruiz, E., et al. 2023, ApJ, 944, 184
Liu, C., Yarza, R., & Ramirez-Ruiz, E. 2025, ApJ, 979, 40
Liu, Z., Ryu, T., Goodwin, A. J., et al. 2024, A&A, 683, L13
Lodato, G., King, A. R., & Pringle, J. E. 2009, MNRAS, 392, 332
Lodato, G., & Rossi, E. M. 2011, MNRAS, 410, 359
Loeb, A., & Ulmer, A. 1997, ApJ, 489, 573
Meza, M. R., Huang, X., Davis, S. W., & Jiang, Y.-F. 2025, arXiv:2506.00109

Miles, P. R., Coughlin, E. R., & Nixon, C. J. 2020, ApJ, 899, 36
Miller, J. M., Kaastra, J. S., Miller, M. C., et al. 2015, Natur, 526, 542
Nicholl, M., Blanchard, P. K., Berger, E., et al. 2019, MNRAS, 488, 1878
Nicholl, M., Lanning, D., Ramsden, P., et al. 2022, MNRAS, 515, 5604
Nixon, C. J., & Coughlin, E. R. 2022, ApJL, 927, L25
Nixon, C. J., Coughlin, E. R., & Miles, P. R. 2021, ApJ, 922, 168
Paczyńsky, B., & Wiita, P. J. 1980, A&A, 88, 23
Pasham, D. R., Lucchini, M., Laskar, T., et al. 2023, NatAs, 7, 88
Pasham, D. R., Remillard, R. A., Fragile, P. C., et al. 2019, Sci, 363, 531
Pasham, D. R., Tombesi, F., Suková, P., et al. 2024, SciA, 10, eadj8898
Pasham, D. R., & van Velzen, S. 2018, ApJ, 856, 1
Paxton, B., Bildsten, L., Dotter, A., et al. 2011, ApJS, 192, 3
Payne, A. V., Shappee, B. J., Hinkle, J. T., et al. 2021, ApJ, 910, 125
Price, D. J., Wurster, J., Tricco, T. S., et al. 2018, PASA, 35, e031
Rees, M. J. 1988, Natur, 333, 523
Ryu, T., Krolik, J., Piran, T., & Noble, S. C. 2020a, ApJ, 904, 98
Ryu, T., Krolik, J., Piran, T., & Noble, S. C. 2020b, ApJ, 904, 99
Ryu, T., Krolik, J., Piran, T., & Noble, S. C. 2020c, ApJ, 904, 101

Sadowski, A., Lasota, J.-P., Abramowicz, M. A., & Narayan, R. 2016, MNRAS, 456, 3915
Shiokawa, H., Krolik, J. H., Cheng, R. M., Piran, T., & Noble, S. C. 2015, ApJ, 804, 85
Smith, L. J., & Gallagher, J. S. 2001, MNRAS, 326, 1027
Springel, V. 2010, MNRAS, 401, 791
Steinberg, E., & Stone, N. C. 2024, Natur, 625, 463
Stone, N., Sari, R., & Loeb, A. 2013, MNRAS, 435, 1809
Tejeda, E., & Rosswog, S. 2013, MNRAS, 433, 1930
van Velzen, S., Gezari, S., Hammerstein, E., et al. 2021, ApJ, 908, 4
Wevers, T., Coughlin, E. R., Pasham, D. R., et al. 2023, ApJL, 942, L33
Wevers, T., Guolo, M., Pasham, D. R., et al. 2024, ApJ, 963, 75
Wevers, T., Pasham, D. R., van Velzen, S., et al. 2019, MNRAS, 488, 4816
Wevers, T., Pasham, D. R., van Velzen, S., et al. 2021, ApJ, 912, 151
Wiseman, P., Williams, R. D., Arcavi, I., et al. 2025, MNRAS, 537, 2024
Wu, S., Coughlin, E. R., & Nixon, C. 2018, MNRAS, 478, 3016
Yao, P. Z., & Quataert, E. 2025, arXiv:2505.10611
Yao, Y., Ravi, V., Gezari, S., et al. 2023, ApJL, 955, L6